Evaluating microstructural parameters of three-dimensional grains generated by phase-field simulation or other voxel-based techniques

2012 Modelling Simul. Mater. Sci. Eng. 20 075009

(http://iopscience.iop.org/0965-0393/20/7/075009)

Modelling Simul. Mater. Sci. Eng. **20** (2012) 075009 (12pp) doi:10.1088/0965-0393/20/7/075009

Evaluating microstructural parameters of three-dimensional grains generated by phase-field simulation or other voxel-based techniques

Kunok Chang[1], Carl E Krill III[2], Qiang Du[1,3] and Long-Qing Chen[1]

[1] Department of Materials Science and Engineering, The Pennsylvania State University, University Park, PA 16802, USA
[2] Institute of Micro and Nanomaterials, Ulm University, 89081 Ulm, Germany
[3] Department of Mathematics, The Pennsylvania State University, University Park, PA 16802, USA

Received 30 January 2012, in final form 23 May 2012
Published 14 September 2012
Online at stacks.iop.org/MSMSE/20/075009

Abstract
The MacPherson–Srolovitz relation expresses the rate of volume change of a grain in a three-dimensional polycrystalline system in terms of microstructural parameters—the mean grain width and the triple line length—as well as isotropic values for the grain boundary mobility and energy. We introduce methods to accurately determine these microstructural measures for grain structures described by a voxel-based microstructure representation, such as those generated by phase-field simulations, Monte Carlo Potts models, or three-dimensional reconstructions of experimentally measured polycrystalline microstructures. We evaluate the mean rate of volume change of grains during a phase-field simulation of grain growth and discuss the results in terms of the MacPherson–Srolovitz relation.

(Some figures may appear in colour only in the online journal)

1. Introduction

Grain growth is one of the most extensively studied processes in materials science, as essentially most engineering materials in use are polycrystalline. Despite the microstructural complexity of such materials, von Neumann and Mullins were able to derive a simple relation between the growth rate of a given grain and its topology that holds for curvature-driven grain growth in 2D: $\mathrm{d}A/\mathrm{d}t = (k\pi/3)(n-6)$, where k is the kinetic constant, A is the area of a grain and n its number of sides [1, 2]. Good agreement was obtained between this equation and experimentally observed kinetics of grain growth observed in thin films of succinonitrile [3]. Phase-field [4, 5], vertex [6] and cellular automaton [7] simulations of two-dimensional grain growth find that the growth rate within each topological class (defined by n) follows the von Neumann–Mullins

relation, although, in the case of phase-field modeling and cellular automata, only on average, rather than for each grain individually.

There have been many attempts to extend the von Neumann–Mullins relation to three dimensions [8–15]. Most notable among these is the recently derived MacPherson–Srolovitz relation,

$$\frac{\mathrm{d}V}{\mathrm{d}t} = -2\pi M\gamma \left(L(D) - \frac{1}{6}\sum_{i=1}^{n} e_i(D) \right), \tag{1}$$

in which V represents the volume of domain D; M and γ denote uniform grain boundary mobility and energy values, respectively, and D is bounded by n triple lines (edges) with lengths $e_i(D)$. $L(D)$ represents the *mean width*, a microstructural measure for the size of the domain [15].

In many cases, the application of equation (1) to microstructures generated by the computer simulation of grain growth requires evaluating mean widths and triple line lengths for grain structures defined on a three-dimensional discrete grid of uniform spacing—i.e. a voxel-based microstructure representation (VBMR). The determination of triple line lengths is also important in its own right for certain practical applications. For example, the total amount of three-phase boundary (TPB) in the cathode of a solid oxide fuel cell is known to play a critical role in its performance, because TPBs are generally believed to be the active sites for the cathode half-cell reactions [16].

For VBMR data, the accurate evaluation of the mean width of a grain and its total triple line length is a challenge, as the discrete nature of the grid leads to an imperfect approximation of any surfaces or linear features that are angled with respect to the voxel faces. Nevertheless, the MacPherson–Srolovitz relation, equation (1), has already been applied to polycrystalline microstructures generated by the Monte Carlo Potts model for grain growth, which employs a VBMR of the simulation cell [8]; however, when carrying out this analysis, Wang and Liu assumed the validity of the relation $E/L = (C_2/6) f^{1/2}$ (with C_2 a constant, E denoting 1/6 of the total length of triple lines bounding a grain, L the grain's mean width, and f its number of faces) instead of directly measuring the triple line length and mean width [8]. On the other hand, the terms on the right-hand side of equation (1) were explicitly evaluated for microstructures generated by 3D vertex models of grain growth [17–19], resulting in good agreement between the growth/shrinkage rate of individual grains calculated according to the MacPherson–Srolovitz relation and the instantaneous rates observed during simulation. But, in this case, the topology of the polycrystalline microstructure is represented by the locations of vertices that are free to take on any positions within the simulation cell, rather than being confined to a discrete grid, as with voxel-based approaches.

In this paper, we present methods for determining the mean width and triple line lengths of grains in VBMRs, such as those underlying Monte Carlo Potts models, phase-field algorithms, or 3D reconstructions of microstructures measured by tomography. As the basis for assessing the accuracy of the methods, we generate three-dimensional polycrystalline microstructures using a multiorder phase-field algorithm for grain growth [20, 21]. Recent progress in improving the efficiency of phase-field models for grain growth includes the optimized algorithm proposed by Gruber *et al* for handling sparse data structures [22] as well as Vanherpe *et al*'s invention of a 'bounding box algorithm' to make larger-scale phase-field simulations feasible [23]. To that same end, boundary-tracking methods were introduced by Kim *et al* [24] and Vedantam and Patnaik [25]; we adopted the latter authors' active parameter tracking (APT) algorithm to enhance computational efficiency and eliminate grain coalescence [25–27].

2. Generation of grain structures

Following [20], a grain structure is described using a set of order parameters $\{\eta_1, \eta_2, \ldots \eta_Q\}$, with each order parameter corresponding to a different grain orientation. We solved the following time-dependent equations for each order parameter,

$$\frac{\partial \eta_i}{\partial t} = -L_i \left(\frac{\delta F}{\delta \eta_i} \right), \qquad i = 1, 2, \ldots, Q, \tag{2}$$

where the L_i denote grain boundary mobilities and F the total free energy of the system. For our simulations, we assumed identical, constant values for all L_i. The free energy is a function of the order parameters and their gradients,

$$F = \int_V \left[f_0(\eta_1, \eta_2, \ldots, \eta_Q) + \frac{1}{2} \sum_{i=1}^{Q} \kappa_i (\nabla \eta_i)^2 \right] \mathrm{d}V, \tag{3}$$

where f_0 represents a local free energy density, and the κ_i are gradient energy coefficients. For a system consisting of many grains, each having one of Q possible orientations, we are free to choose the function f_0 to have degenerate minima at $(\eta_1, \eta_2, \ldots, \eta_Q) = (1, 0, \ldots, 0)$, (0,1,. . .,0), . . ., (0,0,. . .,1). A simple function f_0 satisfying this requirement is given by

$$f_0(\eta_1, \eta_2, \ldots, \eta_Q) = \sum_{i=1}^{Q} \left(-\frac{1}{2} \hat{\alpha} \eta_i^2 + \frac{1}{4} \hat{\beta} \eta_i^4 \right) + \hat{\gamma} \sum_{i=1}^{Q} \sum_{j \neq i}^{Q} \eta_i^2 \eta_j^2, \tag{4}$$

where $\hat{\alpha}$, $\hat{\beta}$ and $\hat{\gamma}$ are phenomenological constants [20]. For $\hat{\alpha} = \hat{\beta} > 0$ and $\hat{\gamma} > \hat{\beta}/2$, f_0 has 2Q minima when $\eta_j = \pm 1$ and $\eta_i = 0$ for all $i \neq j$. Substitution of equations (3) and (4) into equation (2) yields the equation of motion,

$$\frac{\partial \eta_i}{\partial t} = -L_i \left(\hat{\alpha} \eta_i + \hat{\beta} \eta_i^3 + 2 \hat{\gamma} \eta_i \sum_{j \neq i}^{Q} \eta_j^2 - \kappa_i \nabla^2 \eta_i \right). \tag{5}$$

Owing to the implementation of an APT algorithm [25], equation (5) had to be solved only at and near the grain boundaries, a task that was accomplished using a simple forward-Euler integration scheme [20]:

$$\eta_i(t + \Delta t) = \eta_i(t) + \frac{\partial \eta_i}{\partial t} \Delta t + O((\Delta t)^2) \approx \eta_i(t) + \frac{\partial \eta_i}{\partial t} \Delta t. \tag{6}$$

Although the forward-Euler approach lacks the exponential convergence of Fourier spectral methods for solving the equations of motion [28], the adoption of equation (6) was a prerequisite for implementing the APT algorithm.

For the sake of simplicity, we simulated an idealized model system—having uniform grain boundary mobility and energy—rather than a specific polycrystalline material. All parameters of the phase-field model are given in dimensionless units. We performed five sets of three-dimensional simulations with a system size of $240 \times 240 \times 240$ grid points and a grid spacing of $\Delta x = 1.2$, assuming periodic boundary conditions. The coefficients in equation (5) were chosen to be $\hat{\alpha}_i = \hat{\beta}_i = \hat{\gamma}_i = 1, \kappa_i = 2$ and $L_i = 1$ for all i, and the time step Δt in equation (6) was set to 0.1. Under these conditions, each grain boundary in the phase-field simulation spans approximately nine grid points; the kinetics of boundary migration are known to converge to the sharp-interface limit when the smooth change in order-parameter values across the boundary is mapped onto seven or more grid points [29]. We verified that the average grain size $\langle D \rangle$ increased with simulation time according to a power law $\langle D(t) \rangle^n - \langle D(t_0) \rangle^n \propto (t - t_0)$ with initial time t_0; a least-squares fit to the simulated growth curve yielded $n = 1.98$, which is

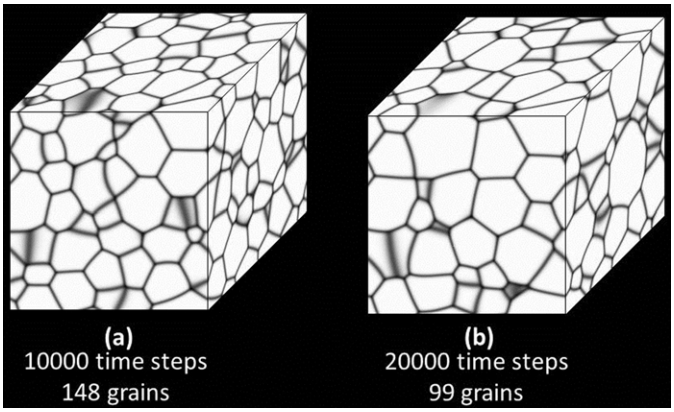

Figure 1. Three-dimensional microstructures generated by phase-field simulation of grain growth performed on a 240^3 simple-cubic grid. The microstructures were visualized by mapping a summation of the squared order-parameter values to a gray scale. (*a*) At 10 000 time steps, 148 grains were present in the simulation cell; (*b*) by 20 000 time steps, the number of grains had dropped to 99.

indistinguishable within statistical error from the parabolic behavior ($n = 2$) that is expected for normal grain growth [20].

At the start of a given simulation run, 320 grains were seeded at randomly chosen locations in the simulation cell. Representative microstructures are shown in figures 1(*a*) and (*b*). Approximately 30 h were required to calculate 40 000 time steps on a personal computer equipped with a dual-core CPU and 2 GB of RAM.

3. Numerical evaluation of microstructural parameters

3.1. Numerical evaluation of mean width

In order to evaluate the right-hand side of the MacPherson–Srolovitz relation, equation (1), we need a method for determining the mean width $L(D)$ of a given grain D [15]. The mean width can be calculated analytically for many shapes, such as spheres and flat-faced polyhedra [15]; however, for an arbitrary domain one must resort to numerical methods, such as the approach proposed in the supplementary information to [15]. The latter method involves determining the surface defined by the grain boundaries enclosing a given grain, triangulating that surface, and measuring the shared edge length (ε_i) and exterior dihedral angle (β_i) between each pair of adjoining triangles in the triangulation. In terms of these quantities, the mean width can be expressed as

$$L(D) = \frac{1}{2\pi} \sum_i \varepsilon_i \beta_i, \tag{7}$$

where β_i is taken to be positive when the surface curvature in the direction perpendicular to the shared edge is convex (with respect to the grain interior), and the summation extends over all shared edges [15].

In a VBMR, the values of the order parameters are known only at the discrete grid points spanning the simulation cell. In order to determine the location of a given grain's surface between grid points, we determined the isosurface for $\eta_i = 0.5$ using the linear interpolation option of the *isosurface* subroutine in MATLAB7 2010a. Perhaps the most popular algorithm

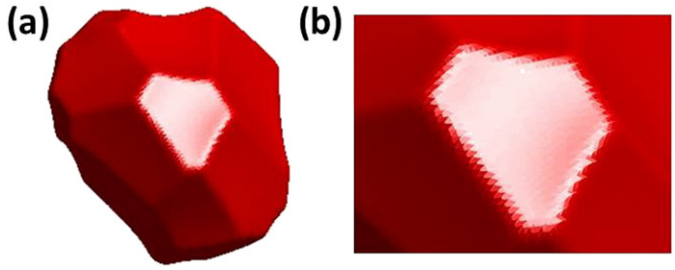

Figure 2. (*a*) Three-dimensional grain generated by phase-field grain growth simulation and visualized using the isosurface subroutine in MATLAB. (*b*) Higher magnification region of (*a*), in which the triangle-based surface mesh is clearly evident.

for isosurface extraction is the Marching Cubes algorithm [30], which returns a surface that is tessellated with triangular regions. The MATLAB subroutine *isosurface* yields tessellations of the same form, but it relies on a custom algorithm that—according to [31]—was written to avoid infringing on the Marching Cubes patent[4]. The subroutine generates an output array listing the vertices comprising each triangle of the isosurface, along with an array containing the coordinates of each of these vertices. The grain itself is provided to the subroutine in the form of a three-dimensional array constructed by allocating a grain orientation to each grid point in the VBMR by selecting the order parameter having the largest value at that voxel: i.e. if η_p is greatest among the order parameters at a certain voxel, the grain orientation at that grid point is p. To achieve a relatively homogeneous mesh size on the isosurface, we imposed a minimum nearest-neighbor separation of $2\Delta x$ on vertices of the isosurface triangulation. Figure 2(*a*) depicts a grain surface obtained in this manner; in the magnified region shown in figure 2(*b*), the triangulation of the isosurface is visible.

From the contents of the array listing the vertices of the isosurface triangles, we can easily determine which triangles share any given edge, and, from the coordinates of each vertex, it is a simple step to calculate the shared edge lengths ε_i. In order to evaluate the exterior dihedral angles β_i between adjacent triangles, we calculate normal vectors to the triangles, choosing the positive direction to point in the outward direction from the enclosed grain, and then define β_i to be the angle between the normal vectors.

In order to assess the accuracy of the mean width calculated by inserting these ε_i and β_i values into equation (7), we examined the cases of tetrahedral, cubic, octahedral and spherical domains (table 1). The 'true' radius of the sphere and the 'true' edge lengths of the polyhedral domains were determined analytically from the measured surface area of each domain and used as the basis for analytic calculation of the mean width [15]. The small relative errors of the numerically evaluated mean widths relative to the analytic values—given in the right-hand column of table 1—validate the applicability of our mesh-based method not only to smoothly bounded domains, such as spheres, but also to domains having abrupt edges.

3.2. Numerical evaluation of triple line length

In addition to the mean width, the right-hand side of equation (1) depends on the lengths of the triple lines bounding the grain whose rate of volume change is being evaluated. Since the

[4] The comparison carried out by Etiene *et al* [32] among a number of isosurfacing packages (primarily variants of the Marching Cubes algorithm) found that the MATLAB algorithm manifests a comparable degree of topological consistency and correctness.

Table 1. Comparison of analytically calculated mean widths (L_{analytic}) to values evaluated numerically (L_{numeric}) for isosurface triangulations of voxel-based representations of selected domain shapes.

Domain D	Surface area	Edge length or radius	Analytically calculated $L_{\text{analytic}}(D)$	Numerically evaluated $L_{\text{numeric}}(D)$	$(L_{\text{numeric}}(D)-L_{\text{analytic}}(D))/L_{\text{analytic}}(D)$ (%)
Tetrahedron	14 854.19	92.61	168.54	179.02	6.2
Cube	8046.18	36.62	109.86	110.16	0.3
Octahedron	33 117.33	97.78	229.77	222.99	−3.0
Sphere	31 399.15	49.99	199.95	203.95	2.0

isosurface extraction procedure described in the previous section was carried out on a grain-by-grain basis, the triple lines were taken into account only to the extent that they modified the surface topography of the grain. (No additional information is needed to calculate the mean width according to equation (7).) This approach does not suffice, however, for determining the lengths of the triple lines, as their locations depend on the positions of the surfaces of neighboring grains, as well. An additional complication is presented by the VBMR itself, which introduces an inherent roughness into the curve along which three grains meet; consequently, the procedure for evaluating triple line lengths must not only identify the voxels bordering three grains simultaneously, but also smooth out any fluctuations arising from the discrete nature of the microstructural representation.

In order to determine which voxels belong to a triple line, we examine the grain orientations of the six nearest-neighbor voxels to each grid point. If the grid point itself has the orientation p and the set of neighboring orientations contains at least two numbers, q and r, differing from each other and from p, then we consider the grid point in question to lie along a triple line. In order to estimate the overall length of a triple line found in this manner more robustly, we perform a principal component analysis (PCA) [33].

The PCA begins by constructing an $N \times 3$ matrix X, consisting of N rows of the voxel coordinates $X_i = (x_i, y_i, z_i)$ associated with the given triple line. Then, we calculate the covariance matrix C of matrix X and determine the eigenvalues and eigenvectors of C. The eigenvector corresponding to the largest eigenvalue is the principal component (P), and each eigenvector is a unit vector. To calculate the lengths Λ_i in figure 3, we take the inner product between X_i and P.

After calculating each $\Lambda_i = X_i \cdot P$, we approximate the triple line length as the difference between the maximum and minimum values of Λ_i (for instance, Λ_2 and Λ_1 in figure 3). Since the PCA method is a statistical approach, its reliability depends on the triple line extending over a sufficient number of voxels to establish its location unambiguously—an implicit assumption of our analysis. In figure 4, we plot the total length of triple lines surrounding individual grains as a function of the cube root of their respective volumes (dividing the triple line length by 6 in accord with the right-hand side of equation (1)). As expected, the larger the grain volume, the longer is the overall triple line length bounding that volume. In the same plot we show the mean width L of each grain calculated according to equation (7). Least-squares fits to $E = \sum_i e_i/6$ and L as a function of $V^{1/3}$ (normalized to the average of the cube root of grain volume) yield the following relations as a function of $x = V^{1/3}/\langle V^{1/3}\rangle$:

$$E = 105.48x^{1.71} + 14.0 \tag{8a}$$

$$L = 24.0x^{1.49} + 97.6 \tag{8b}$$

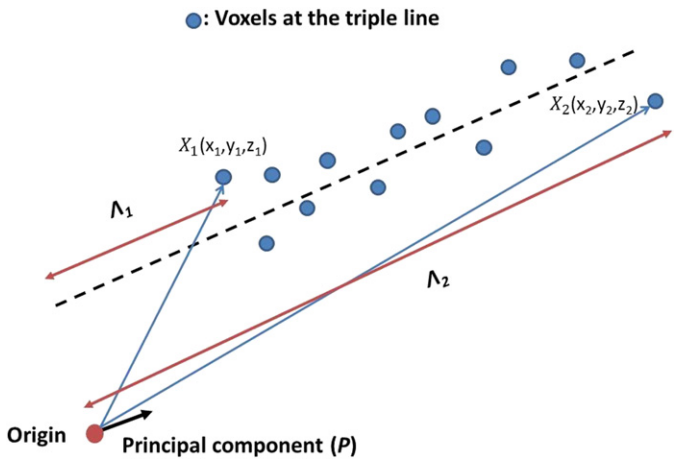

Figure 3. Principle component analysis of a triple line: blue dots mark the locations of voxels at the triple line, and blue arrows indicate the position vectors $X_i = (x_i, y_i, z_i)$, defined relative to the arbitrarily chosen origin (red dot). The lengths Λ_i denote the projections of X_i along the direction of the principal component vector P.

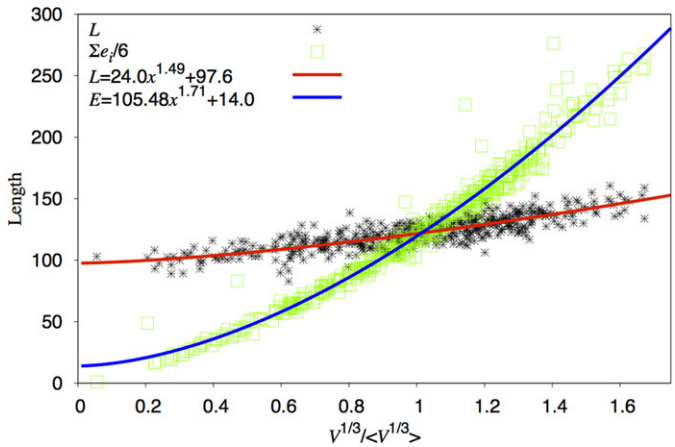

Figure 4. The numerically evaluated mean width L of 459 individual grains and one-sixth of their total triple line lengths, E, both plotted as a function of the normalized cube root of grain volume. This figure includes the results of five separate grain growth simulations, with grain morphologies evaluated after 20 000 time steps.

$$E/\langle E\rangle = 0.84x^{1.71} + 0.11 \tag{8c}$$

$$L/\langle L\rangle = 0.20x^{1.49} + 0.80. \tag{8d}$$

In figure 4, the intersection between the E and L curves defined by equations (8*a*) and (8*b*) is located at approximately $V^{1/3}/\langle V^{1/3}\rangle = 1.015$. Additionally, we note a strong correlation between $V^{1/3}$ and the number of faces f of a grain, as revealed in figure 5; a least-squares fit to these data points yields

$$x = V^{1/3}/\langle V^{1/3}\rangle = 15.34\, f^{0.058} - 16.80. \tag{9}$$

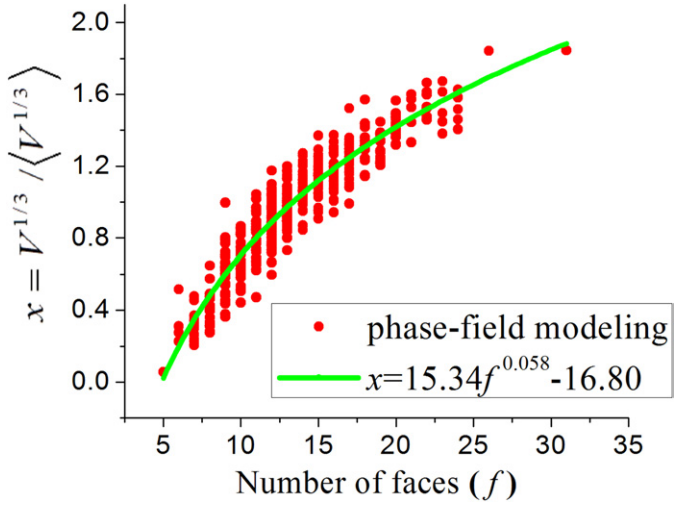

Figure 5. Plot of the normalized cubic root of grain volume against the number of faces (f) for the grains of figure 4.

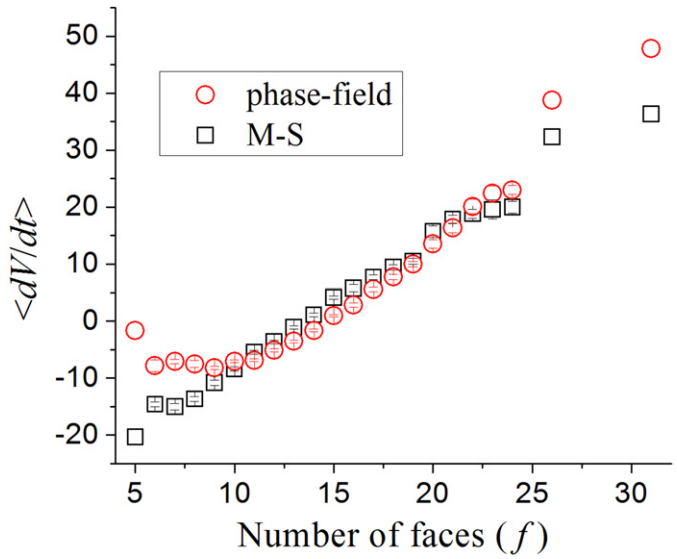

Figure 6. Mean rate of volume change plotted against the number of grain faces f. The MacPherson–Srolovitz ('M-S') volume-change rates were calculated using equation (1), and the 'phase-field' data were obtained from equation (12) applied to grain growth simulations. The vertical bars superimposed on each data point represent the standard deviation of growth rates within the given topological face number class.

Substituting the E/L-crossover value into equation (9) gives $f = 13.2$ for the average face number of grains with zero growth rate, according to the MacPherson–Srolovitz relation. This value is close to the result of an analytic derivation for the coarsening of 3D foams, $f = 13.85$ [34]. Direct measurement of the growth rate as a function of the number of grain faces (figure 6) reveals a slightly larger value of $f \approx 15$ for stagnant grains in our phase-field

simulations, in agreement with vertex modeling [18] and Monte Carlo Potts simulations of grain growth [35]. A recent experimental study of β-Ti found that the integral mean curvature of grain faces vanishes on average at $f = 15.5$, implying zero net growth rate for curvature-driven boundary migration [36].

4. Evaluation of the MacPherson–Srolovitz relation

To test the extent to which the microstructural evolution generated by our phase-field model satisfies equation (1), it is necessary to determine the value of $M\gamma$ for the simulated grain boundaries. This can be performed by measuring the shrinkage rate of a single spherical grain embedded in a uniform matrix and comparing the answer with the analytical solution for curvature-driven grain growth. The assumption that the rate of boundary migration is proportional to the local boundary curvature leads to the expression

$$\frac{\mathrm{d}R}{\mathrm{d}t} = -\frac{2M\gamma}{R}, \tag{10}$$

which links the rate of shrinkage of a spherical grain of radius R to the product of grain boundary mobility M and energy γ [37]. The rate of volume change follows immediately from equation (10):

$$\frac{\mathrm{d}V}{\mathrm{d}t} = 4\pi R^2 \frac{\mathrm{d}R}{\mathrm{d}t} = -4(6\pi^2)^{1/3} M\gamma V^{1/3}. \tag{11}$$

We determine the left-hand side of equation (11) by measuring the volume of the spherical grain at the time steps $t' - \Delta t$ and $t' + \Delta t$ and approximating $\mathrm{d}V/\mathrm{d}t$ at $t = t'$ as

$$\left.\frac{\mathrm{d}V}{\mathrm{d}t}\right|_{t=t'} = \frac{V_{t'+\Delta t} - V_{t'-\Delta t}}{2\Delta t}. \tag{12}$$

The volume at each time step was calculated using the voxel-counting method. Substituting the latter values into equations (11) and (12) yields a value of 0.15 for the quantity $M\gamma$.

Equation (12) was then applied to phase-field simulations of polycrystalline microstructural evolution to obtain quantitative values for the rate of volume change of individual grains during grain growth at 20 000 time steps of the grain growth simulation. The rate of grain volume change can be calculated from the static microstructure at the same time t' using the MacPherson–Srolovitz relation. In figure 6 we compare mean values of the two rates of volume change as a function of the number of grain faces. There is good agreement between the mean growth rates generated by the phase-field model and the predictions of equation (1) for grains having nine or more faces, implying that the methods presented here for evaluating the mean width and the length of triple lines are reasonably accurate.

Since only 7% of the grains in the simulation cell have eight or fewer faces, as revealed by the distribution of the number of faces per grain (figure 7), the discrepancy between simulation and theory is restricted to a small fraction of the sample. Moreover, it is evident in figure 8 that the simulation growth kinetics tend to deviate significantly from the MacPherson–Srolovitz prediction when the rate of volume change of an individual grain drops to values as highly negative as -10. Not only do such rapidly shrinking grains tend to have a low number of faces (figure 6), but, on average, they also tend to be much smaller in size (figure 5), suggesting that the discrepancy between our mesh-based approach and the MacPherson–Srolovitz relation may be traced to inaccuracies in isosurface triangulation and/or triple junction length measurement when characteristic grain dimensions become comparable to the size of the underlying voxels. In this limit, both the linear interpolation that occurs during isosurface extraction and the determination of triple junction lengths via the PCA approach may become problematic, owing

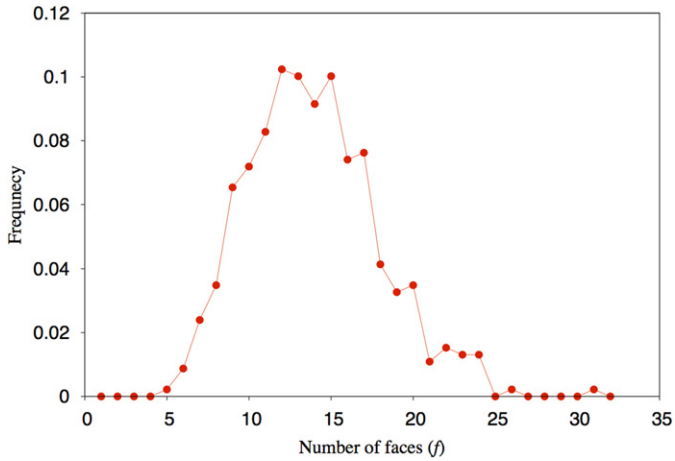

Figure 7. Frequency distribution of the number of faces per grain, calculated from the 459 grains whose microstructural parameters are plotted in figures 4 and 5. Thirty-two of the grains were found to have eight or fewer faces.

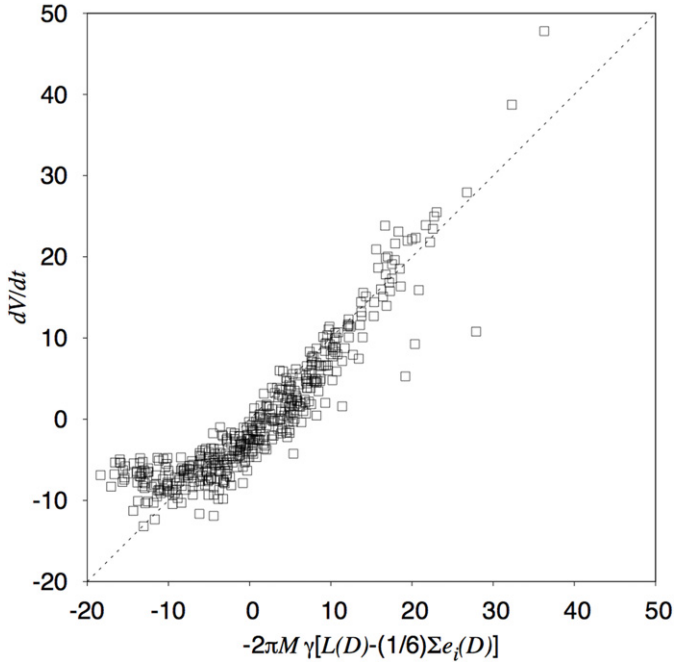

Figure 8. Plot of the rate of volume change of individual grains (open squares)—measured during the phase-field simulation of grain growth—against the growth rate predicted by the MacPherson–Srolovitz relation. The dashed line indicates equality of the measured and predicted values.

to steep gradients in order-parameter values and the small number of voxels located along each triple junction.

Another possible source of error is the effect of the finite width of grain boundaries during phase-field simulation, which causes the grain boundary velocity to deviate from the value

entailed by curvature-driven grain growth when the grain size becomes comparable to the boundary width. Under the simulation conditions of this study, however, such deviations are expected only for grains having, on average, five or fewer faces, which is well below the onset of the discrepancy between the curves plotted in figure 6.

5. Conclusions

We have developed methods for accurately evaluating the mean width and the length of triple lines for three-dimensional grains represented on a uniform, discrete grid. Linear interpolation was adopted to triangulate smooth grain surfaces, and a principal component analysis was employed to estimate the lengths of individual triple lines. For grain growth of a space-filling ensemble of grains, we compared the rates of volume change of individual grains calculated directly by phase-field simulation to the rates predicted by the MacPherson–Srolovitz relation applied to a static microstructure. The mean growth rates obtained by both methods agreed reasonably well for grains having nine or more faces.

Acknowledgments

The authors acknowledge financial support from the National Science Foundation (grant numbers DMR-0710483 and DMS-1016073), CCMD (Center for Computational Materials Design) and the Deutsche Forschungsgemeinschaft through the 'Materials World Network' program. Computing time was provided on instrumentation funded by the National Science Foundation through grant OCI-0821527.

References

[1] Mullins W 1956 *J. Appl. Phys.* **27** 900
[2] von Neumann J 1952 *Metal Interfaces* ed C Herring (Cleveland, OH: American Society for Metals) p 108
[3] Palmer M A, Fradkov V E, Glicksman M E and Rajan K 1994 *Scr. Metall. Mater.* **30** 633
[4] Fan D and Chen L Q 1997 *Acta Mater.* **45** 3297
[5] Fan D, Geng C and Chen L Q 1997 *Acta Mater.* **45** 1115
[6] Weygand D, Brechet Y and Lepinoux J 1998 *Phil. Mag.* B **78** 329
[7] Raghavan S and Sahay S S 2009 *Comput. Mater. Sci.* **46** 92
[8] Wang H and Liu G 2008 *Appl. Phys. Lett.* **93** 131902
[9] Du Q and Le T 2009 *Commun. Math. Sci.* **7** 511
[10] Glicksman M E 2005 *Phil. Mag.* **85** 3
[11] Glazier J A 1993 *Phys. Rev. Lett.* **70** 2170
[12] Mullins W and Vinals J 1989 *Acta Metall.* **37** 991
[13] Hilgenfeldt S, Kraynik A M, Reinelt D A and Sullivan J M 2004 *Europhys. Lett.* **67** 484
[14] Cahn J W 1967 *Trans. Met. Soc. AIME* **239** 610
[15] MacPherson R D and Srolovitz D J 2007 *Nature* **446** 1053 and supplementary information
[16] Kim J W, Virkar A V, Fung K Z, Mehta K and Singhal S C 1999 *J Electrochem. Soc.* **146** 69
[17] Syha M and Weygand D 2010 *Modelling Simul. Mater. Sci. Eng.* **18** 015010
[18] Mora L A B, Gottstein G and Shvindlerman L S 2008 *Acta Mater.* **56** 5915
[19] Lazar E A, Mason J K, MacPherson R D and Srolovitz D J 2011 *Acta Mater.* **59** 6837
[20] Krill C E III and Chen L Q 2002 *Acta Mater.* **50** 3057
[21] Chen L Q and Yang W 1994 *Phys. Rev.* B **50** 15752
[22] Gruber J, Ma N, Wang Y, Rollett A D and Rohrer G S 2006 *Modelling Simul. Mater. Sci. Eng.* **14** 1189
[23] Vanherpe L, Moelans N, Blanpain B and Vandewalle S 2007 *Phys. Rev.* E **76** 056702
[24] Kim S G, Kim D I, Kim W T and Park Y B 2006 *Phys. Rev.* E **74** 061605
[25] Vedantam S and Patnaik B S V 2006 *Phys. Rev.* E **73** 016703
[26] Chang K, Feng W and Chen L Q 2009 *Acta Mater.* **57** 5229
[27] Suwa Y, Saito Y and Onodera H 2007 *Acta Mater.* **55** 6881

[28] Chen L Q and Shen J 1998 *Comput. Phys. Commun.* **108** 147
[29] Fan D, Chen L Q and Chen S P 1997 *Mater. Sci. Eng.* A **238** 78
[30] Lorensen W and Cline H 1987 *SIGGRAPH Comput. Graph.* **21** 163
[31] Zask R and Dailey M N 2009 *6th Int. Conf. ECTI-CON (Pattaya, Chonburi)* p 672
[32] Etiene T, Scheidegger C, Nonato L G, Kirby R M and Silva C 2009 *IEEE Trans. Visual. Comput. Graph.* **15** 1227
[33] Jolliffe I T 1986 *Principal Component Analysis* 2nd edn (New York: Springer)
[34] Hilgenfeldt S, Kraynik A M, Koehler S A and Stone H A 2001 *Phys. Rev. Lett.* **86** 2685
[35] Streitenberger P and Zöllner D 2006 *Scr. Mater.* **55** 461
[36] Rowenhorst D J, Lewis A C and Spanos G 2010 *Acta Mater.* **58** 5511
[37] Hillert M 1965 *Acta Metall.* **13** 227